Liu, R., & Ding, Z. (2017). Stability of viscous film flow coating the interior of a vertical tube with a porous wall. *Physical Review E*, *95*(5), [053101]. https://doi.org/10.1103/PhysRevE.95.053101

Stability of viscous film flow coating the interior of a vertical tube with a porous wall

Rong Liu*
School of Mechanical and Electrical Engineering, Gui Lin University of Electronic Technology, Gui Lin 541004, China

Zijing Ding†
School of Mathematics, University of Bristol, Bristol BS8 1TW, United Kingdom

(Received 1 February 2017; revised manuscript received 30 March 2017; published 1 May 2017)

The stability of the gravity-driven flow of a viscous film coating the inside of a tube with a porous wall is studied theoretically. We used Darcy's law to describe the motion of fluids in a porous medium. The Beaver-Joseph condition is used to describe the discontinuity of velocity at the porous-fluid interface. We derived an evolution equation for the film thickness using a long-wave approximation. The effect of velocity slip at the porous wall is identified by a parameter β. We examine the effect of β on the temporal stability, the absolute-convective instability (AI-CI), and the nonlinear evolution of the interface deformation. The results of the temporal stability reveal that the effect of velocity slip at the porous wall is destabilizing. The parameter β plays an important role in determining the AI-CI behavior and the nonlinear evolution of the interface. The presence of the porous wall promotes the absolute instability and the formation of the plug in the tube.

DOI: 10.1103/PhysRevE.95.053101

I. INTRODUCTION

A liquid film flowing down the inner or outer wall of a vertical cylinder has received extensive attention because it is encountered in many industrial applications and biological phenomena [1]. The exterior flow on a fiber is associated with technological applications, such as draining, the coating of insulation on a wire, and the protective coating of tube walls [2]. The interior flow on a tube occurs in many applications, such as lung airways [3,4] and oil recovery by water injection [5].

In recent years, most of the attention has been focused on the problem of exterior coating flow on a cylindric fiber. An experimental investigation of thin films flowing down a vertical fiber was performed first by Quéré [6]. The results showed that two different kinds of behaviors can be observed depending on the film thickness: (i) For a thick film on a slender fiber, drops develop due to the Rayleigh mechanism [7] and they flow downward. Some of the drops grow by swallowing the other ones and they quickly fall, leaving behind a thick film that breaks in turn into droplets. (ii) For a thin film on a large fiber, the instability may be arrested by the mean flow.

Several modeling approaches have been developed to investigate the dynamics of exterior coating flows on fibers. These models can be loosely categorized into three groups: (i) thin-film asymptotic models, (ii) long-wave asymptotic models, and (iii) integral models. The first models are derived to study the flow in which the ratio between film thickness (h) and cylinder radius (a) is small. Frenkel derived a simple Benney-like equation for the evolution of the film thickness using a thin-film approximation [8]. The nonlinear dynamics of Frenkel's equation has also been investigated by Kalliadasis and Chang [9], Kerchman and Frenkel [10], and Chang and Demekhin [11].

Kliakhandler, Davis, and Bankoff [12] conducted experiments that revealed the richness of the dynamics of the flow down a vertical fiber. In their experiments, the film is at least twice as thick as the fiber radius. Therefore, the previously derived Benney-like equation under the assumption of $h \ll a$ does not apply there. The authors proposed an evolution equation that does not rely on the previously made thin-film assumptions. Craster and Matar [13] derived a new evolution equation similar to that used by Kliakhandler, Davis, and Bankoff [12], and they revisited the same problem in which the fluid radius is much smaller than its characteristic length based upon a capillary length scale.

All of the modeling attempts described above assumed negligible inertia effects. Therefore, they are only valid for small Reynolds numbers of Re $\sim O(1)$. Ruyer-Quil *et al.* [14] formulated a two-equation model for the film thickness h and flow rate q using a weighted residuals approach. This model, accounting for inertia and streamwise viscous diffusion, is valid for moderate Reynolds numbers, both small and $O(1)$ aspect ratios of h/a. Comparisons between the numerical and experimental results show good agreement in both the linear and nonlinear regimes.

The interior coating flow falls in the class of core-annular flows where the gas phase occupies the core and a viscous fluid occupies the annulus between the tube wall and the core. The most critical difference between the film dynamics of the exterior and the interior coating flow is that for the interior case the film may form occlusive liquid plugs in the tube. Camassa *et al.* [15] studied, both experimentally and theoretically, flows where a viscous liquid film lining the inside of a tube is forced upward against gravity by turbulent air flow up the center of the tube. Ring waves were identified as a mass transport mechanism in air-driven core-annular flows. Camassa *et al.* [16] have studied the linear stability and the nonlinear evolution of a viscous film falling down a vertical tube driven by gravity. The results of linear stability analysis indicate that for any tube size there exists a film thickness large enough to become absolutely unstable. The results of numerical simulation predict a critical film thickness that leads to the formation of plugs in the tube. More recently, Camassa and Ogrosky [17] performed a theoretical and numerical

*rongliu@guet.edu.cn
†z.ding@bristol.ac.uk

investigation of two classes of models, namely "long-wave" and "thin-film" models, for pressure-driven core-annular flow. The authors examined their dynamical differences with respect to the asymptotic assumptions made in the process of model derivation. Dietze and Ruyer-Quil [18] considered the axisymmetric arrangement of an annular liquid film, coating the inner surface of a narrow cylindrical tube, in interaction with an active core fluid. The authors derived a simplified second-order low-dimensional model by applying the weighted residual integral boundary layer (WRIBL) approach to both fluid phases, fully taking into account inertia as well as axial viscous diffusion and full interphase coupling.

The instability of a falling film on a porous wall is a natural extension of the problem of a falling film flowing on an impermeable wall. Such problems have been given extensive attention in recent years. Pascal [19] first investigated the linear stability of a Newtonian fluid flowing down an inclined permeable plane. In Ref. [19], Darcy's law together with the Beavers-Joseph condition [20] is used to describe flow in a porous medium. However, the author made an assumption that $K/h^2 \ll 1$ such that the flow in the porous medium can be neglected, where K is the permeability and h is the thickness of the fluid film. The effect of a porous medium on the dynamics of the combined layers is described by a slippery boundary condition. Thus, a one-sided model [19], in which the dynamics of the fluid layer and the porous layer has been decoupled, has been proposed to study the dynamics of the film. The one-sided model has been widely used in many recent papers on the stability of falling films on porous inclines [21–23]. In mathematical form, this one-sided model is identical to that of the problem of a film falling down a slippery inclined plane [24]. Liu and Liu [25] proposed a two-sided model by giving up the assumptions in Ref. [19], and they solved the coupled equations for both the liquid and the porous medium rather than the one-sided equation. A linear stability analysis has been performed by solving the eigenvalue problem of the Orr-Sommerfeld equations. A comparison of the results of the two-sided model with that of the one-sided model indicates that the one-sided model is qualitatively valid, and the results of these two models are very close because the permeability of the porous medium is very low. In the two-sided model by Liu and Liu [25], Darcy's equation and the Beavers-Joseph condition are used to describe the dynamics of the flow. Similar two-sided models in which the porous medium is governed by the Darcy-Brinkman equations and other sets of boundary conditions are employed in several recent works [26,27].

Recently, Ding and Liu [28] and Ding *et al.* [29] studied the stability of a liquid film coating the outside a porous cylinder. In this work, we will study the dynamics of the gravity-driven flow of a viscous film coating the interior porous wall of a vertical tube. The present paper is organized as follows. In Sec. II, a mathematical formulation of the physical model is presented. In Sec. III, we present the results and discussions. In Sec. IV, we summarize the results and present the conclusions.

II. MATHEMATICAL FORMULATION

As shown in Fig. 1, a Newtonian fluid, of constant viscosity μ and density ρ, flows down a porous wall of a tube with the inner radius $r = a$ under gravity g. The initial radius of the fluid surface measured from the center of the fiber is $r = R_0$. The mean thickness of the film is denoted by $h_0 = a - R_0$. The free surface is located at $r = S(z,t)$.

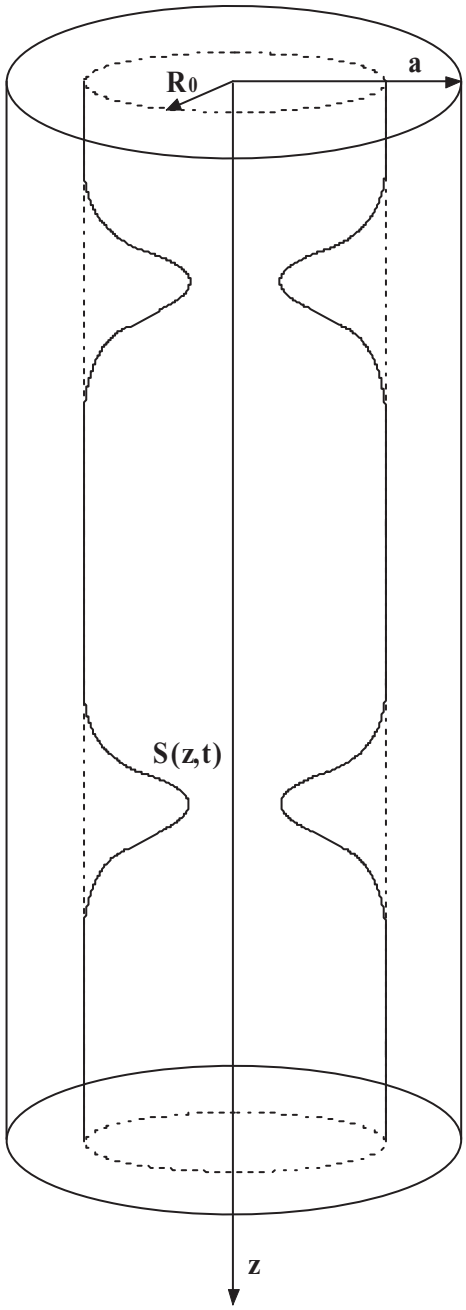

FIG. 1. Sketch of the geometry of film flow coating the interior of the tube.

The dynamics of the axisymmetric flow of the film is governed by the Navier-Stokes equations,

$$u_r + \frac{u}{r} + w_z = 0, \tag{1}$$

$$u_t + uu_r + wu_z = -\frac{p_r}{\rho} + \frac{\mu}{\rho}\left[u_{rr} + \frac{u_r}{r} - \frac{u}{r^2} + u_{zz}\right], \tag{2}$$

$$w_t + uw_r + ww_z = g - \frac{p_z}{\rho} + \frac{\mu}{\rho}\left[w_{rr} + \frac{w_r}{r} + w_{zz}\right], \tag{3}$$

where t denotes time, u and w denote the radial (r) and axial (z) velocity components, and p denotes the pressure. Note that unless stated otherwise, the subscript denotes partial differentiation.

The porous medium is assumed to be saturated with fluid, and the flow in it is assumed to be governed by Darcy's law. The flow velocity in the porous medium

$$w^m = -\frac{K}{\mu}(p_z - \rho g), \tag{4}$$

where the permeability K has dimensions of (length)^2 and the superscript m denotes the porous medium.

At the fluid-porous interface ($r = a$), the boundary conditions include the Beavers-Joseph condition [20]

$$w_r = -\frac{\alpha}{\sqrt{K}}(w - w^m), \tag{5}$$

and the continuity of the axial velocities,

$$u = u^m, \tag{6}$$

where α is a dimensionless parameter dependent on the structure of the porous medium, and (u^m, w^m) is the Darcian mean filter velocity in the porous medium.

We use V to denote the axis velocity scale, and l and h_0 to denote the axis and radius length scale, respectively. In the thin liquid film, the pressure scale is

$$P \sim \frac{\mu V l}{h_0^2}, \tag{7}$$

and the velocity scale of w^m is

$$V^m \sim \frac{KV}{h_0^2}. \tag{8}$$

If the pore space geometry is such that the magnitude of flow velocity in the porous medium is much slower than V, i.e., $K/h_0^2 \ll 1$, then the mean filter velocities are negligible. Using these approximations in the boundary conditions at the fluid-porous interface, we have

$$w_r = \frac{\alpha}{\sqrt{K}}w, \tag{9}$$

$$u = 0. \tag{10}$$

Thus, the dynamic of the flow in the porous medium can be decoupled from that of the fluid layer [19].

At the free surface $r = S(z,t)$, the balance of shear stress,

$$\boldsymbol{t}\cdot\boldsymbol{T}\cdot\boldsymbol{n} = \boldsymbol{0}, \tag{11}$$

and the normal stress balanced by surface tension times the curvature,

$$\boldsymbol{n}\cdot\boldsymbol{T}\cdot\boldsymbol{n} = 2\sigma H, \tag{12}$$

are required, where $\boldsymbol{T}$ is the stress tensor, $\boldsymbol{n}$ and $\boldsymbol{t}$ are the unit vectors normal and tangent to the interface, σ is the surface tension, and $2H$ is the sum of the principal curvatures.

In component form, Eqs. (11) and (12) can be expressed as

$$2S_z(u_r - w_z) + (1 - S_z^2)(w_r + u_z) = 0, \tag{13}$$

$$p^g - p + \frac{2\mu}{N^2}[-S_z(u_z + w_r) + u_r + S_z^2 w_z] = \sigma\left(\frac{1}{NS} - \frac{S_{zz}}{N^3}\right), \tag{14}$$

where $N = (1 + S_z^2)^{1/2}$, and p^g is the background pressure.

The kinematic condition at the free surface is

$$S_t + wS_z - u = 0, \tag{15}$$

or in conservative form

$$S_t + \frac{1}{S}\frac{\partial}{\partial z}\int_a^S wr\,dr = 0. \tag{16}$$

A. Scaling and asymptotic reduction

We render the governing equations dimensionless by adopting the following scalings:

$$r = h_0\bar{r},\ z = l\bar{z},\ p = \rho g l\bar{p},\ t = lV^{-1}\bar{t},$$
$$w = V\bar{w},\ u = \epsilon V\bar{u}, \tag{17}$$

where the velocity scale $V \equiv \rho g h_0^2/\mu$, and the bar indicates that the variables are dimensionless. We choose the thickness of undisturbed film, h_0, as the radial length scale. The axial length scale, l, is taken to be related to the capillary length, $\sigma/\rho g R_0$.

The dimensionless Navier-Stokes equations are

$$u_r + \frac{u}{r} + w_z = 0, \tag{18}$$

$$\epsilon^3\mathrm{Re}(u_t + uu_r + wu_z) = -p_r + \epsilon^2\left[u_{rr} + \frac{u_r}{r} - \frac{u}{r^2} + \epsilon^2\frac{\partial^2 u}{\partial z^2}\right], \tag{19}$$

$$\epsilon\,\mathrm{Re}(w_t + uw_r + ww_z) = 1 - p_z + \left[w_{rr} + \frac{w_r}{r} + \epsilon^2 w_{zz}\right], \tag{20}$$

where the Bond number $\mathrm{Bo} = \rho g h_0^2/\sigma$, the Reynolds number is defined as $\mathrm{Re} = \rho^2 g h_0^3/\mu^2$, and $\epsilon = h_0/l$. For simplicity, we have dropped the bar for all the dimensionless variables. Assuming $\epsilon \ll 1$ and $\mathrm{Re} \sim O(1)$, we can remove the contributions of the inertial terms. We consider the relative sizes of the parameters for experiments conducted by Camassa *et al.* [16], in which $\mathrm{Re} \sim O(10^{-2})$ or smaller. Thus, even as $\epsilon \sim O(10^{-1})$, we also take $\epsilon\,\mathrm{Re} \to 0$, and we can neglect the inertial term.

The leading-order Navier-Stokes equation is given by

$$p_r = 0, \tag{21}$$

$$w_{rr} + \frac{w_r}{r} = p_z - 1. \tag{22}$$

The leading-order tangential and normal stress balances at the surface are

$$w_r = 0 \tag{23}$$

and

$$p = -\frac{\epsilon}{\mathrm{Bo}}\left(\frac{1}{S} - \epsilon^2 S_{zz}\right). \tag{24}$$

The terms in parentheses in Eq. (24) model the role that surface tension plays through the azimuthal and axial curvature in an axisymmetric film. A notable term that is included in Eq. (24) is the S_{zz} term, which involves the highest derivative of S. Strictly speaking, the inclusion of this term may appear to be ad hoc. The contribution of the streamwise curvature $\epsilon^2 S_{zz}$ due to surface tension must be kept in our formulation as it is well known from the planar case that this is the principal physical effect that prevents the waves from breaking. The importance of the role of this item is reflected in a linear analysis in which the inclusion of this term is vital to ensure that the correct high-wave-number cutoff occurs. Conventionally, this term is kept in long-wave theories of jets, threads, and liquid bridges [13,30].

At the fluid-porous interface, the Beavers-Joseph condition is

$$-\beta w_r = w, \tag{25}$$

in which $\beta = \frac{\sqrt{K}}{\alpha h_0}$ is the dimensionless parameter describing the influence of velocity slip at the the porous-fluid interface. In the experiments by Beavers and Joseph [20], α has the values 0.78, 1.45, and 4.0 for a metal having an average pore size of 0.016, 0.034, and 0.045 in., respectively. The film thickness in the present problem has a magnitude of 0.1 cm. Values of K for natural materials vary widely. Typical values for soils are 10^{-9}–10^{-10} and for clean gravel 10^{-7}–10^{-9}. In this paper, the value of β ranges from 0.1 to 0.4.

Solving Eq. (22), we have $w = (1 - p_z)(-\frac{r^2}{4} + c\ln r + d)$, in which c and d are two undetermined coefficients. Substituting w into Eqs. (23) and (25), we have c and d as

$$c = \frac{S^2}{2},\ d = \frac{1}{4}\eta^2 - \frac{1}{2}S^2\ln\eta + \frac{\beta}{2\eta}(\eta^2 - S^2). \tag{26}$$

Lastly, we obtain the expression of w as

$$w = (1 - p_z)\left[\frac{1}{4}(\eta^2 - r^2) + \frac{1}{2}S^2\ln\frac{r}{\eta} + \frac{\beta}{2\eta}(\eta^2 - S^2)\right], \tag{27}$$

in which $\eta = \frac{a}{h_0}$ denotes the dimensionless radius of the porous wall. We can define the flow rate Q as

$$Q(S) = \int_\eta^S r w\, dr. \tag{28}$$

The flow rate Q is expressed as

$$\begin{aligned} Q(S) &= \int_\eta^S r w\, dr \\ &= (1 - p_z)\left[\frac{1}{4}S^4\log\frac{S}{\eta} + \frac{(3S^2 - \eta^2)(\eta^2 - S^2)}{16}\right. \\ &\quad \left. - \frac{\beta}{4\eta}(\eta^2 - S^2)^2\right]. \end{aligned} \tag{29}$$

Substituting Q in the kinematic boundary condition yields an evolution equation for $S(z,t)$ given by

$$\partial_t S^2 + 2\partial_z Q(S) = 0. \tag{30}$$

III. RESULTS AND DISCUSSIONS

A. Temporal stability analysis

Let us now consider the linear stability of the problem. The base state of Eq. (27) is

$$S_0 = \eta - 1. \tag{31}$$

We use a normal mode approach in which the basic state of the interface is slightly perturbed by a Fourier mode,

$$S = S_0 + \hat{S}\exp(\lambda t + ikz), \tag{32}$$

where $\hat{S}$ is the amplitude of the perturbation, and k and λ are the wave number and the (complex) temporal growth rate. This yields a dispersion relation

$$\begin{aligned} S_0\lambda = {} & \frac{\epsilon}{16\mathrm{Bo}}k^2\left(k^2\epsilon^2 - \frac{1}{S_0^2}\right) \\ & \times\left(4S_0^4\ln\frac{S_0}{\eta} - \eta^4 + 4S_0^2\eta^2 - 3S_0^4 - 4\frac{\beta}{\eta}\left(\eta^2 - S_0^2\right)^2\right) \\ & - \frac{ik}{2}\left(S_0\eta^2 - S_0^3 + 2S_0^3\ln\frac{S_0}{\eta} - \frac{2\beta}{\eta}S_0\left(S_0^2 - \eta^2\right)\right). \end{aligned} \tag{33}$$

We use $\mathrm{Re}(\lambda)$ and $\mathrm{Im}(\lambda)$ to denote the real and imaginary parts of λ. $\mathrm{Re}(\lambda)$ and $\mathrm{Im}(\lambda)$ correspond to its growth or decay rate and the frequency of the disturbance. The phase speed of the disturbance is defined as $c = -\frac{\mathrm{Im}(\lambda)}{k}$. In Eq. (33), the wave speed c is positive and independent of the wave number k. This means all disturbances with different wave numbers propagate downstream at the same speed.

To know the effect of β on the growth rate, it is helpful to analyze the sign of the factor

$$4S_0^4\ln\frac{S_0}{\eta} - \eta^4 + 4S_0^2\eta^2 - 3S_0^4 - 4\frac{\beta}{\eta}\left(\eta^2 - S_0^2\right)^2 \tag{34}$$

in Eq. (33). It can be shown straightforwardly that the term $4S_0^4\ln\frac{S_0}{\eta} - \eta^4 + 4S_0^2\eta^2 - 3S_0^4$ is negative and the term $(\eta^2 - S_0^2)^2$ is positive. The cutoff wave number at which the real growth rate is zero is

$$k_c = \frac{1}{\epsilon S_0}. \tag{35}$$

As $0 < k < k_c$, the growth rate is positive. For each unstable mode with a fixed k, both the growth rate $\mathrm{Re}(\lambda)$ and the phase speed c increase with the increase of β. This means that the presence of a porous wall makes the film more unstable and makes the disturbance propagate faster downstream.

We call the disturbance with the maximum real growth rate λ_m the "most unstable mode." The maximum real growth rate,

$$\begin{aligned} \lambda_m = {} & \frac{-1}{64\epsilon\mathrm{Bo}S_0^5}\left(4S_0^4\ln\frac{S_0}{\eta} - \eta^4 + 4S_0^2\eta^2 - 3S_0^4\right. \\ & \left. - 4\frac{\beta}{\eta}\left(\eta^2 - S_0^2\right)^2\right), \end{aligned} \tag{36}$$

is realized at the wave number

$$k_m = \frac{1}{\sqrt{2}\epsilon S_0}. \tag{37}$$

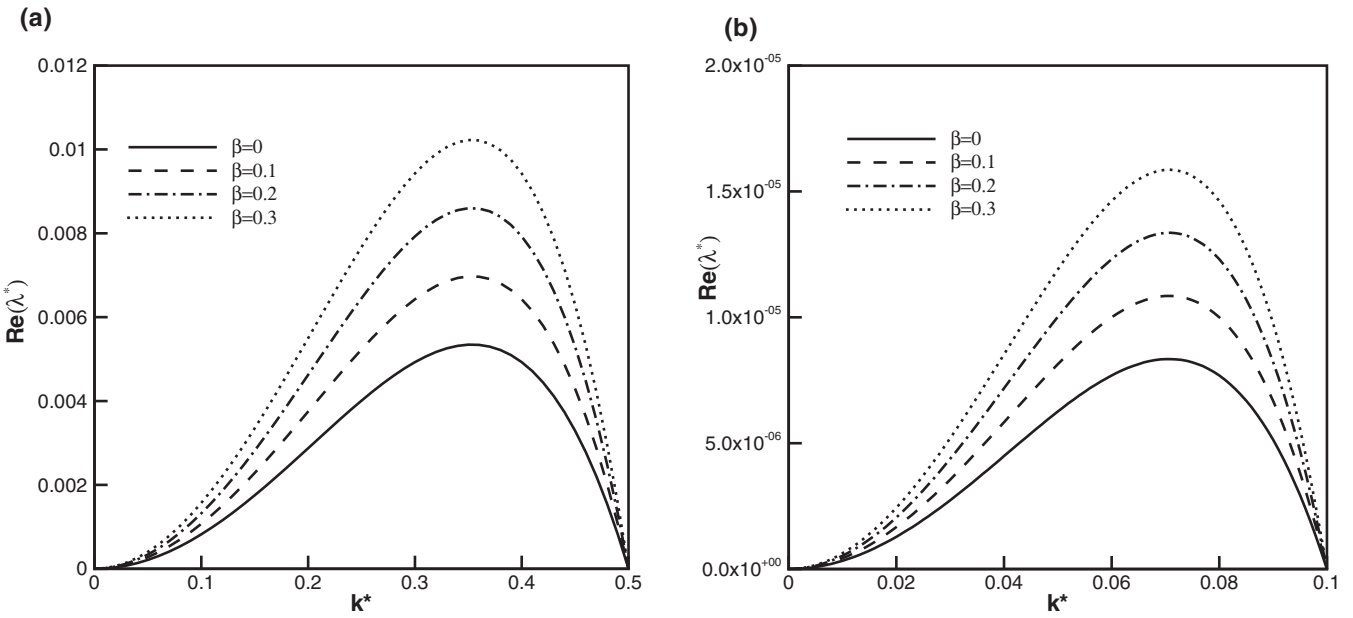

FIG. 2. The dispersion relation of the real growth rate vs the wave number for various β. (a) For $\eta = 3$, (b) for $\eta = 11$. k^* and λ^* are the modified wave number and time-growth rate defined as $k^* = \epsilon k$, $\lambda^* = \epsilon \mathrm{Bo}\lambda$.

Rescaled by S_0, the wave number of the "most dangerous mode" and the cutoff wave number are identical to the exterior case [13]. Both of the disturbances with wave numbers of k_c and k_m are short waves. Strictly speaking, they lie outside the range of validity of the long-wave model. This originates from the inclusion of the curvature term $\epsilon^2 S_{zz}$ in Eq. (24). Being similar to the exterior case, the cutoff wave number corresponds to the classical Rayleigh-Plateau mode for the capillary instability of a viscous jet.

To know quantitatively the effect of velocity slip at the porous wall on the stability, we plot the curves of the growth rate versus the wave number for various β. In Fig. 2, $\eta = 3$ and 11 correspond to relatively thicker and thinner films. In the range of $0 < k < k_c$, with the increases of β the growth rate increases remarkably. As β increases from 0 to 0.3, the maximal growth rate of $\beta = 0.3$ increases to about a time above that of $\beta = 0$.

In Fig. 3, we plot the curves of the maximal growth rate and the phase speed c versus η for various β. As shown in Fig. 3(a), the maximal growth rate decreases with the increase of η. With the increase β, the maximal growth rate of the most unstable mode increases. In Fig. 3(b), for thicker films

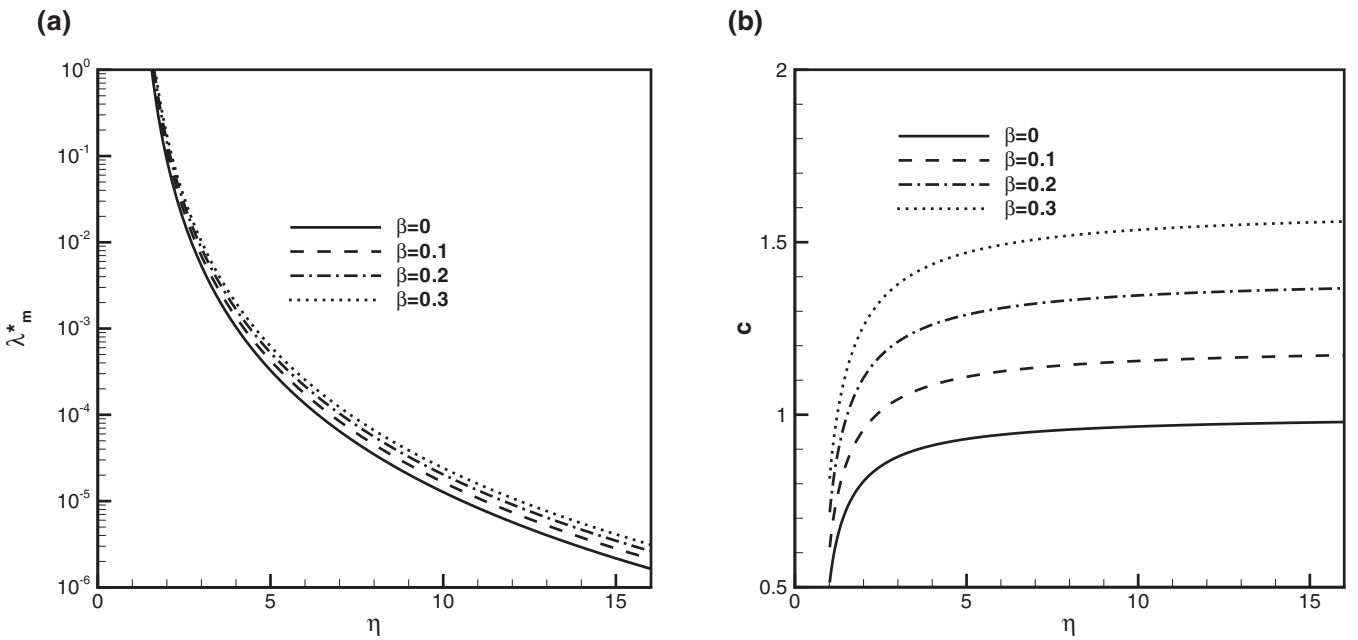

FIG. 3. (a) The maximum growth rate vs η for various β. (b) The phase speed c of disturbance vs η for various β.

the wave speed c increases remarkably with the increase of η. For thinner films, the wave speed increases gradually with the increase of η. With the increase of β, the wave speed increases at each η.

B. Spatiotemporal analysis: Absolute and convective instabilities

In open-flow hydrodynamic systems, instabilities can be either convective or absolute. If localized disturbances spread upstream and downstream and contaminate the entire flow region, the system is locally absolutely unstable. By contrast, if the disturbances are swept away from the source, the system is locally convectively unstable. The concept of the absolute-convective instability (AI-CI) was first developed in the context of plasma physics [31,32] and later it was extended to the problems of hydrodynamics [34].

In experiments, the AI-CI characteristics can be categorized by the location where instability growth can be visually detected. In the present problem, films that only exhibit visible instability growth far away from the inlet, and those that exhibit growth very near the inlet, are classified as convectively unstable and absolutely unstable, respectively.

In this subsection, we carry out a spatiotemporal stability analysis, and consequently both the wave number k and the frequency ω will be complex numbers. For a general hydrodynamics stability problem, the wave number and frequency satisfy a dispersion relation of the form

$$\mathscr{D}(k,\omega) = 0. \tag{38}$$

The stability properties of the perturbations were determined by studying the long-time behavior of an impulsive response to a localized excitation. The solution of the impulsive response can be expressed in the form

$$G(x,t) = \frac{1}{2\pi}\int_A\int_F \frac{e^{i(kx-\omega t)}}{\mathscr{D}(k,\omega)}d\omega\, dk, \tag{39}$$

where the Bromwich contour F in the ω plane is a horizontal line lying above all the singularities to satisfy causality, and the integration path A lies inside the analyticity band around the k axis.

To distinguish between convective and absolute instabilities, it is necessary to examine the long-time behavior of the wave number k_0 along the ray x/t at a fixed spatial location. This complex k_0 has, by definition, a zero group velocity

$$\frac{\partial\omega}{\partial k}(k_0) = 0, \tag{40}$$

and $\omega_0 = \omega(k_0)$ is called the absolute frequency. If $\mathrm{Im}(\omega_0) > 0/\mathrm{Im}(\omega_0) < 0$, the instability is said to be absolutely and convectively unstable. It should be noted that the saddle point k_0 used to identify absolute and convective instability must satisfy the Briggs-Bers [31,33] collision criterion, i.e., the saddle point must be a pinch point produced by two distinct spatial branches of solutions of the dispersion relation coming from the upper and lower half-k planes. The method to study the absolute and convective instability is a standard procedure. For more details on AI-CI problems, we refer the reader to a good review article by Huerre and Monkewitz [34]. Duprat *et al.* [35] have studied the absolute and convective instability of an exterior coating film on a vertical fiber both experimentally and theoretically. The most relevant work on our problem is the study of the AI-CI characteristics of an interior coating film down a vertical tube [16].

Camassa *et al.* [16] have conducted a series of experiments to study the gravity-driven film coating the interior of a vertical tube. In their experiments, tubes of three different inner radii were used for the experiments: 5×10^{-3}, 2.95×10^{-3}, and 1.7×10^{-3} m. The liquid used was a silicone oil with dynamic viscosity $\mu = 12.9\ \mathrm{N\,s/m^2}$, density $\rho = 970\ \mathrm{kg/m^3}$, and surface tension $\sigma = 2.15\times10^{-2}\ \mathrm{N\,m^{-1}}$. In the present paper, we used the same set of parameters as that used in Ref. [16].

The dispersion relation of the present problem is

$$\omega = \frac{1}{16\epsilon \mathrm{Bo} S_0}\left\{i\epsilon^2k^2\left(\frac{1}{S_0^2}-\epsilon^2k^2\right)f_1(\eta,\beta)+\epsilon k f_2(\eta,\beta)\right\}, \tag{41}$$

in which

$$f_1 = -\left(4S_0^4\ln\frac{S_0}{\eta}-\eta^4+4S_0^2\eta^2-3S_0^4-4\frac{\beta}{\eta}\left(\eta^2-S_0^2\right)^2\right), \tag{42}$$

$$f_2 = \frac{1}{2}\left(S_0\eta^2-S_0^3+2S_0^3\ln\frac{S_0}{\eta}-\frac{2\beta}{\eta}S_0\left(S_0^2-\eta^2\right)\right). \tag{43}$$

Through the transformation $\tilde{k} = \alpha^{-1}k$, $\tilde{\beta} = (\epsilon\alpha S_0)^{-2}$, and $\tilde{\omega} = (16\epsilon\mathrm{Bo}\alpha^{-1}f_2^{-1})\omega$, where $\alpha = \epsilon^{-1}[f_2/(3f_1)]^{1/3}$, the dispersion relation reduces to a standard form as

$$\tilde{\omega} = \tilde{k} + \frac{i\tilde{k}^2}{3}(\tilde{\beta}-\tilde{k}^2). \tag{44}$$

A straightforward analysis based on (44) then shows that the instability becomes absolute when $\tilde{\beta} > \tilde{\beta}_c = [(9/4)(-17+7\sqrt{7})]^{1/3}$ [35]. Therefore, applying $\tilde{\beta} = (\epsilon\alpha S_0)^{-2}$ to the condition $\tilde{\beta} > \tilde{\beta}_c$ yields the following implicit condition for absolute instability:

$$\left(\frac{3f_1}{f_2}\right)^{2/3} > \tilde{\beta}_c S_0^2. \tag{45}$$

The contour plot of the complex temporal growth rate for a typical value of $\hat{\beta} = \hat{\beta}_c$ is shown in Fig. 4. There are three saddle points given by the condition $d\tilde{\omega}/d\tilde{k} = 0$ in the complex k plane in Fig. 4. One saddle point, $\tilde{k}_1$, in the upper half-plane is a pure imaginary number. This point does not satisfy the Briggs criterion since it is produced by two distinct branches coming from the upper plane. The other two saddle points, $\tilde{k}_{2,3}$, are pinch points produced by two distinct branches coming from the upper and lower planes.

To know the AI-CI characteristics of the film, we examined the pinch point for each pair point in the (a,R_0) plane as $a \leqslant 0.005$ m. Figure 5 shows the boundaries between the regimes of absolute and convective instabilities in the (a,R_0) plane for various β. Each curve in Fig. 5 shows that for relatively thin films the instability is convective. For a fixed a, there is a critical inner radius R_c below which the instability becomes absolute. Fixing R_0 and increasing a, or fixing a and decreasing

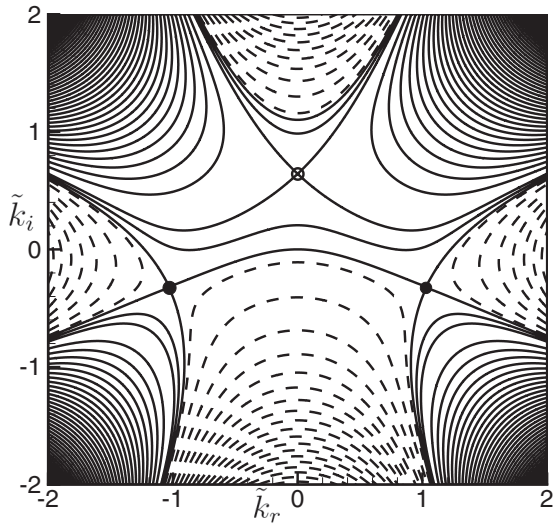

FIG. 4. Contour lines of $\tilde{\omega}_i$ in the complex $\tilde{k}$ plane for $\tilde{\beta} = \tilde{\beta}_c \approx 1.507$. Positive and negative values of $\tilde{\omega}_i$ are denoted by solid and dashed lines. The three saddle points are $\tilde{k}_1 \approx 0.643i$ (marked by a hollow circle) and $\tilde{k}_{2,3} = \pm 1.031 - 0.321i$ (marked by solid circles). The points $\tilde{k}_{2,3}$ satisfy the Briggs criterion.

R_0, promotes the absolute instability. For a given a, it is found that with the increase of β, the critical R_c increases. This means that the presence of the porous wall promotes the absolute instability.

C. Nonlinear evolution

In this subsection, we study the nonlinear evolution from a perturbed initial state. Equation (30) subject to periodic boundary conditions was solved numerically. The solution is approximated by the Fourier series:

$$S(z,t) = \sum_{-N/2}^{N/2} \hat{s}_n(t) \exp\left[i \frac{2\pi n z}{L}\right], \tag{46}$$

where $s_n(t)$ is the time-dependent coefficient, N is the number of Fourier modes, and L is the computational length. A Fourier pseudospectral method is used to provide the discretization in space. An implicit Gears method for stiff problems was used for the time advance, and the relative error is set less than 10^{-6}.

Camassa *et al.* [16] performed numerical simulations on the long-wave model for a thin film coating the interior of the tube. The results showed that for film with a mean thickness smaller than some critical value depending on a, i.e., $h_0 < h_c(a)$, these instabilities saturate as a series of small-amplitude traveling waves. For thicker films with $h_0 > h_c(a)$, there is numerical evidence that the model can break down with some form of finite-time blowup. Near the blowup time, the interface deformation with the largest amplitude undergoes rapid growth to the point of becoming comparable to the tubes radius, i.e., $S(z,t) = 0$. As $S(z,t)$ approaches zero, some of the coefficients of the long-wave model equation become large, leading to a very stiff problem in which the numerical simulation usually breaks down. The authors have not provided a full mathematical characterization of this blowup trend. It is natural to take the tendency for the interface location S to approach zero as an indication of the formation of a plug. The authors compared this "choke" criterion for plug formation based on the numerical simulation with the experimental observation. Experimental films with a mean thickness smaller than some critical value very close to what the theoretical model predicts do not exhibit plug formation, while thicker films do.

In this subsection, we will study the effect of velocity slip at the porous wall on the nonlinear evolution of small disturbances. We now examine the nonlinear evolution initiated by small disturbances of the most unstable modes with a wavelength of $2\pi/k_m$. The initial condition is a simple harmonic disturbance superimposed on the interface:

$$S(0,z) = S_0 + \varepsilon \cos(k_m z). \tag{47}$$

The computational domain is set to be the interval $[-\pi/k_m, \pi/k_m]$. In Fig. 6, we plot the profiles of the saturated state of the nonlinear evolution initiated by small disturbances of the most unstable modes for several typical parameters. Figure 6 shows that no blowup behavior has been observed for the given parameters. At the saturated state, the interface evolves into a series of traveling waves. Because the traveling waves are steady, we only need to plot a time snapshot as the evolution reaches the saturated state. In Fig. 6, it is found that with the increase of β, the amplitude of the wave increases. As R_0 decreases to a critical value, the blowup behavior begins to be observed.

In Fig. 7, the points of traveling waves and the "choke" points determined by the blowup criterion are marked by squares and triangles. At a small radius of $a = 0.001$ m, the boundary between the plug and no-plug regimes is very close to the AI-CI boundary. For larger a, this boundary is higher than the AI-CI boundary. In Fig. 7, it is found that in the regime of absolute instability, the blowup behavior always occurs. Comparing Fig. 7(a) with Fig. 7(b), it is found that

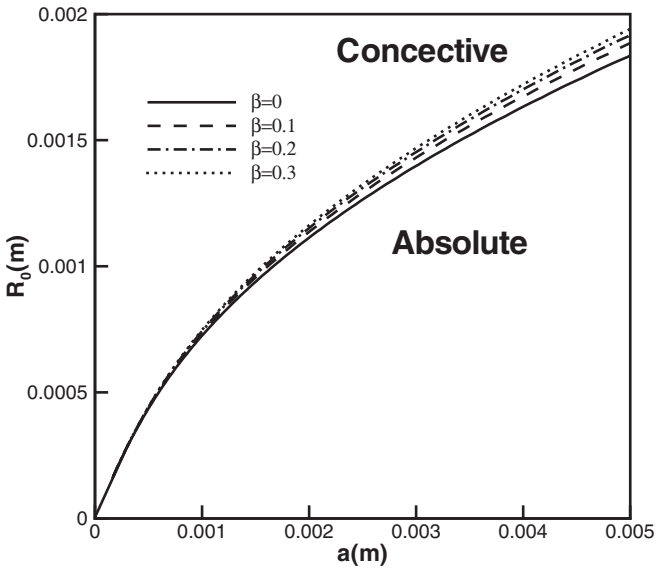

FIG. 5. The boundaries between the convective and absolute instabilities for various β.

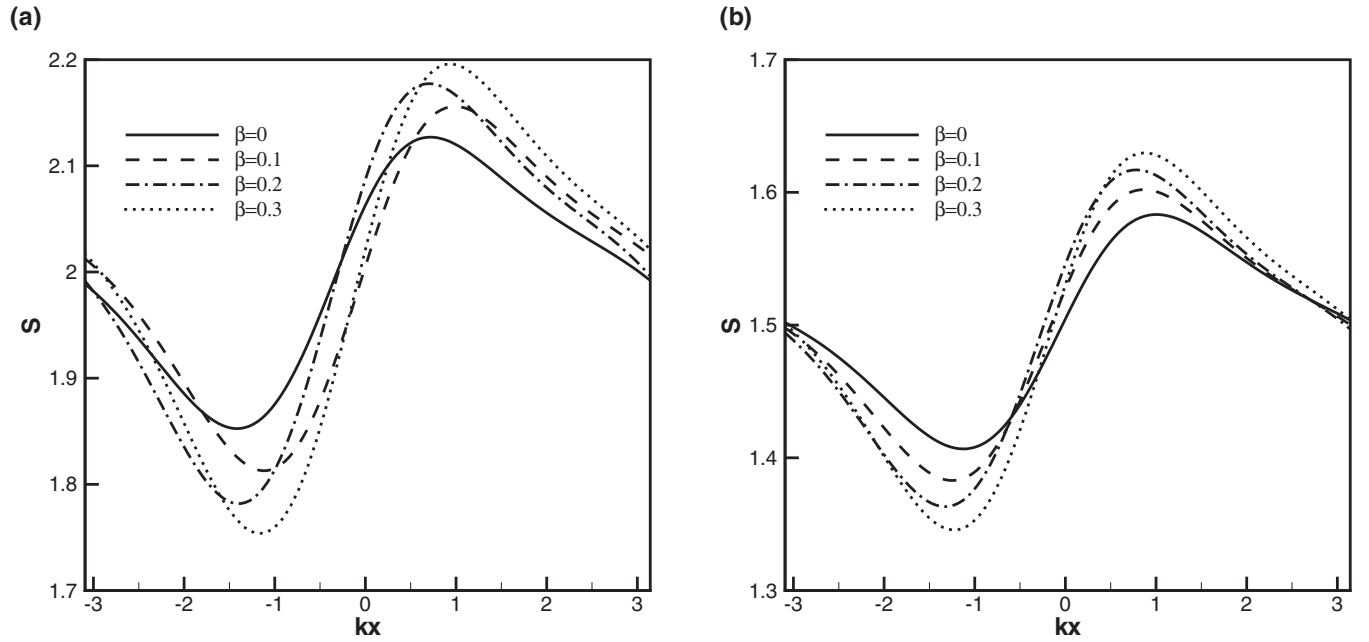

FIG. 6. Effect of β on the profiles of the interface via numerical simulations for the most unstable disturbances. Other parameters are (a) $a = 0.003$ m and $R_0 = 0.002$ m, and (b) $a = 0.005$ m and $R_0 = 0.003$ m.

with the increase of β, the plug and no-plug boundary extends to the thinner film regimes in the a-R_0 plane. For example, at $a = 0.005$ m, the value of R_0 is 0.002 52 and 0.002 65 m for $\beta = 0$ and 0.2, respectively. This result means that with the increase of β, at the nonlinear state the profile of the interface may change from a traveling wave to a plug flow.

To know the properties of the solutions that are naturally selected, we perform numerical simulations on relatively long domains for several typical sets of parameters. Starting from a coating flow of uniform radius seeded with most unstable disturbances with an amplitude in the range of $0–10^{-3}$ on a spatial domain with a length of $10\pi k_m^{-1}$, the profiles of the free surface are plotted in Fig. 8. In Fig. 8(a), the parameters $\beta = 0$, $a = 0.005$ m, and $R_0 = 0.0027$ m are located in the no-plug regime as shown in Fig. 7(a). After a long-time evolution, the film reaches a quasi-steady-state regime and the profile of the interface is in the form of a series of traveling waves. As β increases to 0.2, the interface undergoes rapid growth

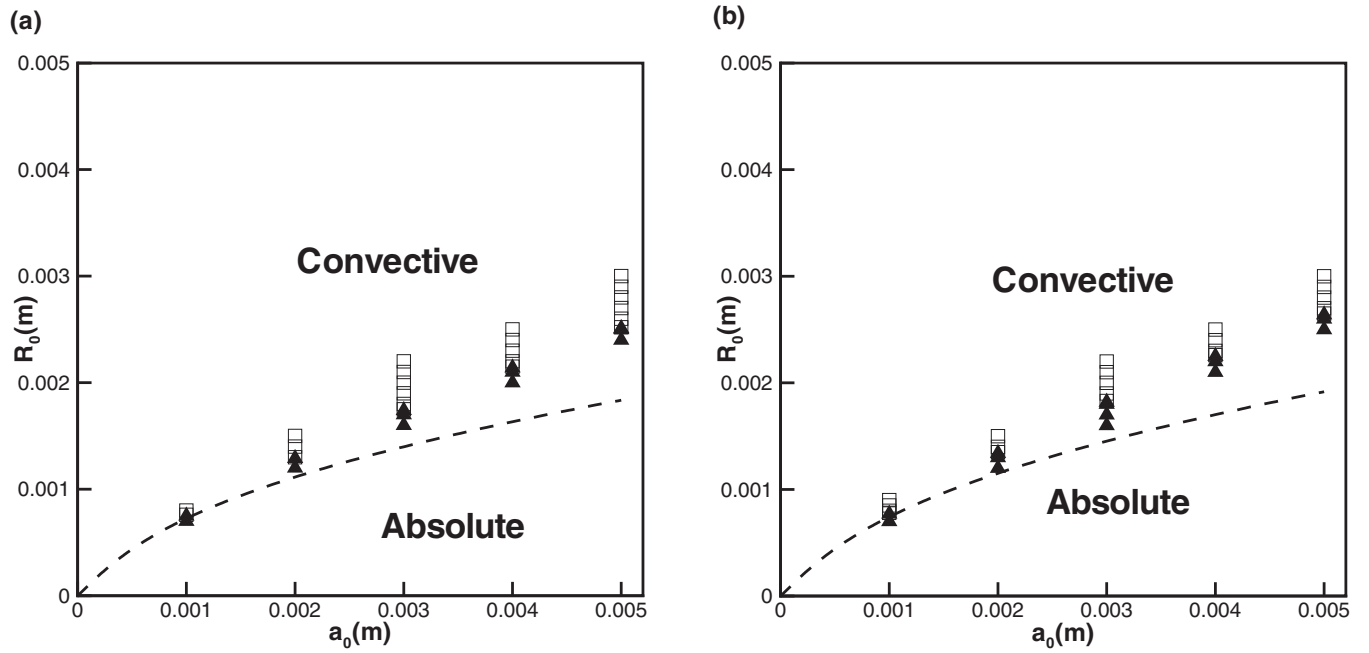

FIG. 7. Parametric space for mean interfacial thickness R_0 and tube radius a. Plug and no-plug regions are marked by squares and triangles. The boundaries between the AI-CI regimes are plotted by dashed lines. (a) $\beta = 0$, (b) $\beta = 0.2$.

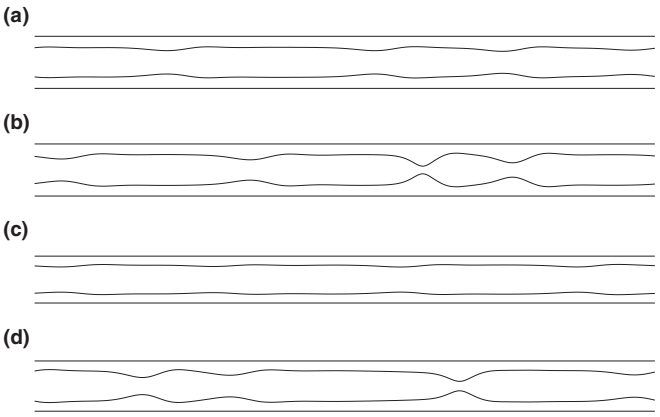

FIG. 8. The profiles of the interface via numerical simulations on the long-wave model equation (30) for various parameters. (a) $\beta = 0$, $R_0 = 0.0027$ m; (b) $\beta = 0.2$, $R_0 = 0.0027$ m; (c) $\beta = 0.2$, $R_0 = 0.003$ m; and (d) $\beta = 0.4$, $R_0 = 0.0028$ m. Other parameters are $a = 0.005$ m and $\epsilon = 0.2$.

to the point of becoming $S = 0$. Figure 8(b) shows the profile of the interface before blowup. After a very short time of evolution, the liquid will choke the tube and form a liquid plug. Fixing $\beta = 0$, $a = 0.005$ m, and increasing $R_0 = 0.003$ m, the blowup behavior disappears. As shown in Fig. 8(c), the interface consists of a series of quasisteady traveling waves. As β increases to 0.4 and R_0 decreases to $R_0 = 0.0028$ m, a blowup behavior occurs. As shown in Fig. 8(d), the profile of the interface before blowup is similar to Fig. 8(b).

IV. CONCLUSIONS

We have carried out a theoretical investigation on gravity-driven flows of viscous films coating the inside of a vertical tube with a porous wall. Darcy's law with the Beaver-Joseph condition is used to describe the flow in a porous medium and the discontinuity of velocity at the porous-fluid interface. An evolution equation has been derived based on long-wave asymptotics. The effect of velocity slip at the porous wall is identified by a parameter β.

We studied the linear stability and nonlinear evolution of the problem. The result of linear stability shows that with the increase of β, the growth rate and the phase speed of disturbances of unstable modes increase. We also studied the absolute and convective instability characteristics via spatiotemporal analysis. The results showed that for relatively thin films, the instability is convective. For a fixed a, there is a critical inner radius R_c below which the instability becomes absolute. The critical value R_c of the boundary between the convective and absolute instabilities increases with the increase of β. This means that the effect of velocity slip at the porous wall promotes the absolute instability.

We performed numerical simulations on the nonlinear evolution. The critical film mean thickness beyond which the plug interface will be formed is sought by examining the blowup behavior of the evolution equation. We examine the formation of a plug for several typical parameters as $a = 0.001$–0.005 m. At a small radius of $a = 0.001$ m, the boundary between the plug and no-plug regimes is very close to the AI-CI boundary. For larger a, this boundary is higher than the AI-CI boundary in the (a, R_0) plane. With the increase of β, the critical mean film thickness of the plug and no-plug boundaries decreases. This result means that the increase of β promotes the formation of the plug interface.

ACKNOWLEDGMENT

This work was supported by the National Natural Science Foundation of China (Grant No. 11102211).

[1] S. J. Weinstein and K. J. Ruschak, Coating flows, Annu. Rev. Fluid Mech. **36**, 29 (2004).
[2] D. Quéré, Fluid coating on a fiber, Annu. Rev. Fluid Mech. **31**, 347 (1999).
[3] J. B. Grotberg, Pulmonary flow and transport phenomena, Annu. Rev. Fluid Mech. **26**, 529 (1994).
[4] J. B. Grotberg, Respiratory fluid mechanics, Phys. Fluids. **23**, 021301 (2011).
[5] K. L. Olbricht, Pore-scale prototypes of multiphase flow in porous media, Annu. Rev. Fluid Mech. **28**, 187 (1996).
[6] D. Quéré, Thin films flowing on vertical fibers, Europhys. Lett. **13**, 721 (1990).
[7] L. Rayleigh, On the instability of a cylinder of viscous liquid under capillary force, Philos. Mag. **34**, 145 (1892).
[8] A. L. Frenkel, Nonlinear theory of strongly undulating thin films flowing down vertical cylinders, Europhys. Lett. **18**, 583 (1992).
[9] S. Kalliadasis and H.-C. Chang, Drop formation during coating of vertical fibres, J. Fluid Mech. **261**, 135 (1994).
[10] V. I. Kerchman and A. L. Frenkel, Interactions of coherent structures in a film flow: Simulations of a highly nonlinear evolution equation, Theor. Comput. Fluid Dyn. **6**, 235 (1994).
[11] H.-C. Chang and E. A. Demekhin, Mechanism for drop formation on a coated vertical fibre, J. Fluid Mech. **380**, 233 (1999).
[12] I. L. Kliakhandler, S. H. Davis, and S. G. Bankoff, Viscous beads on vertical fibre, J. Fluid Mech. **429**, 381 (2001).
[13] R. V. Craster and O. K. Matar, On viscous beads flowing down a vertical fibre, J. Fluid Mech. **553**, 85 (2006).
[14] C. Ruyer-Quil, P. Treveleyan, F. Giorgiutti-Dauphiné, C. Dupat, and S. Kalliadasis, Modelling film flows down a fibre, J. Fluid Mech. **603**, 431 (2008).
[15] R. Camassa, M. G. Forest, L. Lee, H. R. Ogrosky, and J. Olander, Ring waves as a mass transport mechanism in air-driven core-annular flows, Phys. Rev. E **86**, 066305 (2012).
[16] R. Camassa, H. R. Ogrosky, and J. Olander, Viscous film flow coating the interior of a vertical tube. Part 1. Gravity-driven flow, J. Fluid Mech. **745**, 682 (2014).
[17] R. Camassa and H. R. Ogrosky, On viscous film flow coating the interior of a vertical tube: Thin-film and long-wave models, J. Fluid Mech. **772**, 569 (2015).
[18] G. F. Dietze and C. Ruyer-Quil, Films in narrow tubes, J. Fluid Mech. **762**, 68 (2015).

[19] J. P. Pascal, Linear stability of fluid flow down a porous inclined plane, J. Phys. D **32**, 417 (1999).
[20] G. S. Beavers and D. D. Joseph, Boundary conditions at a naturally permeable wall, J. Fluid Mech. **30**, 197 (1967).
[21] J. P. Pascal, Instability of power-law fluid flow down a porous incline, J. Non-Newtonian Fluid Mech. **133**, 109 (2006).
[22] I. M. R. Sadiq and R. Usha, Thin Newtonian film flow down a porous inclined plane: Stability analysis, Phys. Fluids **20**, 022105 (2008).
[23] R. Liu and Q. S. Liu, Instabilities and transient behaviors of a liquid film flowing down a porous inclined plane, Phys. Fluids **22**, 074101 (2010).
[24] A. Samanta, C. Ruyer-Quil, and B. Goyeau, A falling film down a slippery inclined plane, J. Fluid Mech. **684**, 353 (2011).
[25] R. Liu and Q. S. Liu, Instabilities of a liquid film flowing down an inclined porous plane, Phys. Rev. E **80**, 036316 (2009).
[26] U. Thiele, B. Goyeau, and M. Velarde, Stability analysis of thin film flow along a heated porous wall, Phys. Fluids **21**, 014103 (2009).
[27] R. Usha and S. Naire, A thin film on a porous substrate: A two-sided model, dynamics and stability, Chem. Eng. Sci. **89**, 72 (2013).
[28] Z. J. Ding and Q. S. Liu, Stability of liquid films on a porous vertical cylinder, Phys. Rev. E **84**, 046307 (2011).
[29] Z. J. Ding, T. N. Wong, R. Liu, and Q. S. Liu, Viscous liquid films on a porous vertical cylinder: Dynamics and stability, Phys. Fluids **25**, 064101 (2013).
[30] J. Eggers and T. F. Dupont, Drop formation in a one-dimensional approximation of the Navier-Stokes equation, J. Fluid Mech. **262**, 205 (1994).
[31] R. J. Briggs, *Electron-Stream Interaction with Plasmas* (MIT Press, Cambridge, MA, 1990).
[32] A. Bers, *Linear Waves and Instabilities*, in *Physique des Plasmas*, edited by C. DeWitt and J. Peyraud (Gordon & Breach, New York, 1975).
[33] A. Bers, *Space-time Evolution of Plasma Instabilities—Absolute and Convective*, in *Handbook of Plasma Physics*, edited by M. N. Rosenbluth and R. Z. Sagdeev (North-Holland, Amsterdam, 1983).
[34] P. Huerre and P. A. Monkewitz, Local and global instabilities in spatially developing flows, Annu. Rev. Fluid Mech. **22**, 473 (1990).
[35] C. Duprat, C. Ruyer-Quil, S. Kalliadasis, and F. Giorgiutti-Dauphiné, Absolute and Convective Instabilities of a Viscous Film Flowing Down a Vertical Fiber, Phys. Rev. Lett. **98**, 244502 (2007).